CHAPTER IV

RESULTS AND DISCUSSION

The EtOAc extract of the grayish black Thai marine sponge *Pachastrissa nux* was found to exhibit strong antifungal activity against *Candida albicans* ATCC 10231. The EtOAc layer was then dissolved in MeOH and partitioned with hexane. The crude MeOH extract was further chromatographed on a SiO_2 gel vacuum column, a Sephadex LH-20 column, a SiO_2 gel flash column, and a preparative HPLC to give three active compounds, kabiramides C, D, and F. Kabiramides C, D, and F were obtained as white amorphous solids in 1.07×10^{-2} , 2.54×10^{-4}, and 0.91×10^{-4} % wet weight, respectively.

1. Identification and structure elucidation of the isolated kabiramides

The structures of the isolated kabiramides were elucidated by analyses of NMR, MS, UV, and IR spectroscopic data, together with comparison with the literatures.

1.1 Identification of kabiramide C

Kabiramide C was obtained as a white amorphous solid. The ESI mass spectrum (Figure 38) established the pseudomolecular ion peak at *m/z* 964.4866 $[M+Na]^+$ implying the molecular formula of $C_{48}H_{71}N_5O_{14}$. The UV spectrum (Figure 39) exhibited the absorption at λ_{max} 247 nm corresponding to three consecutive oxazole rings conjugating with a double bond. The IR absorption at 3455 cm^{-1} indicated the presence of hydroxy and/or amine groups while the presence of ester and amide groups were implied by bands at 1716 and 1653 cm^{-1}, respectively (Figure 40). This compound showed specific rotation $[\alpha]^{23}_D$ + 8.33° (*c* 0.047, $CHCl_3$).

The ^{1}H NMR spectrum (in $CDCl_3$, Figure 41) showed the characteristic peaks of trisoxazole macrolides including three singlet protons of three oxazole rings at δ 8.09 (H-14), 8.03 (H-17), and 7.57 (H-11) ppm; double singlets of *N*-formamide protons at δ 8.27 and 8.06 ppm; double singlets of *N*-methyl proton signals at δ 3.02 and 3.06 ppm; double doublets of olefinic (H-35) at δ 6.45 and 7.11 ppm; and a doublet of olefinic proton (H-34) at δ 5.09 ppm. The double signals of some protons appeared in the ratio of 2:1 due to the two geometrical forms of the *N*-formyl group. The ^{1}H NMR spectrum also exhibited some proton signals that were characteristic of kabiramide compounds such as six methyl proton signals (δ 1.14, 0.98, 0.92, 0.90, 0.86, and 0.81 ppm), four methoxy proton signals (δ 3.44, 3.42, 3.33, and 3.31 ppm), and two olefinic proton signals (δ 7.45 and 6.28 ppm) (Table 8).

The ^{13}C NMR spectrum (Figure 42) also displayed some double carbon signals, in the ratios of 2:1, i.e. C-29 (δ 42.33 and 42.26 ppm), C-30 (δ 213.70 and 213.79 ppm), C-31 (δ 48.98 and 49.07 ppm), C-32 (δ 87.14 and 87.22 ppm), C-33 (δ 37.52 and 37.58 ppm), C-34 (δ 111.16 and 112.93 ppm), C-35 (δ 128.49 and 124.48 ppm), 35-NCH_3 (δ 27.59 and 33.10 ppm), and 35-NCHO (δ 161.86 and 160.59 ppm). The complete assignments of ^{13}C NMR spectrum are shown in Table 8.

The H,H COSY spectrum (Figure 45) revealed the consecutive proton connectivity as follows: H-2/H-3/H-4/H-5/5-CH_3/H-6/H-7/H-8/8-CH_3, H-9/H-11, H-19/H-20/H-21/H-22, H-23/CH_3-23, H-24/H-25/H-26/H-27/27-CH_3/H-28/H-29/H-31, H-33/33-CH_3 and H-34/H-35 (Figure 15).

The one-bond connected protons and carbons were assigned by HMQC spectrum (Figure 44) as summarized in Table 8. The HMBC spectrum ($^{n}J_{HC}$ = 8 Hz, Figures 46-47) revealed the long range correlations between each fragments and the position of methoxy groups as shown in Figure 15. The HMBC spectrum also showed the position of carbons in each oxazole rings. The *N*-methyl formamide was connected to C-35 by the observed correlation from the *N*-methyl protons to C-35. Additionally, the chemical shift of H-24 at δ 5.14 ppm suggested that the ester group was attached at C-24.

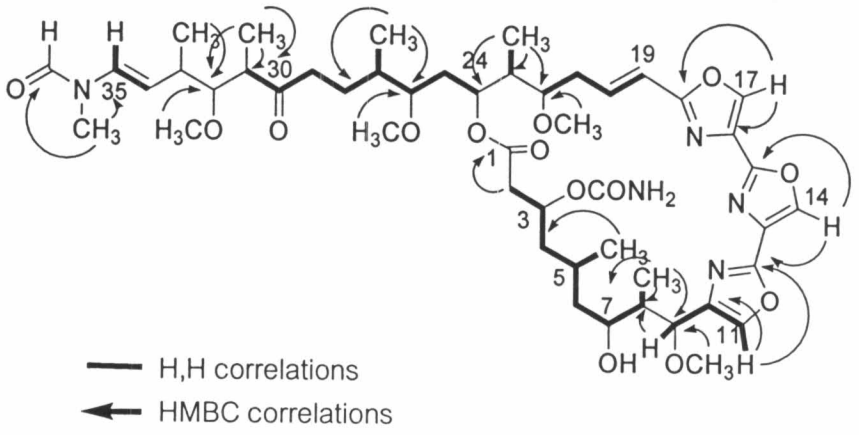

Figure 15 The H,H correlations (bold line) and HMBC correlations (arrow) of kabiramide C.

The absolute stereochemistry of the kabiramide C was determined by X-ray structure of Ca-ATP form of G-actin in complex with kabiramide C at a resolution of 1.45 Å (Klenchin et al., 2003). The absolute stereochemistry of the chiral centers was defines as 3*S*, 5*R*, 7*S*, 8*S*, 9*R*, 22*S*, 23*R*, 24*S*, 26*S*, 27*S*, 31*R*, 32*R*, 33*R* as shown in Figure 16. Kabiramide C was previous isolated from nudibranch *Hexabranchus* sp. egg masses (Matsunaga et al., 1986; 1989).

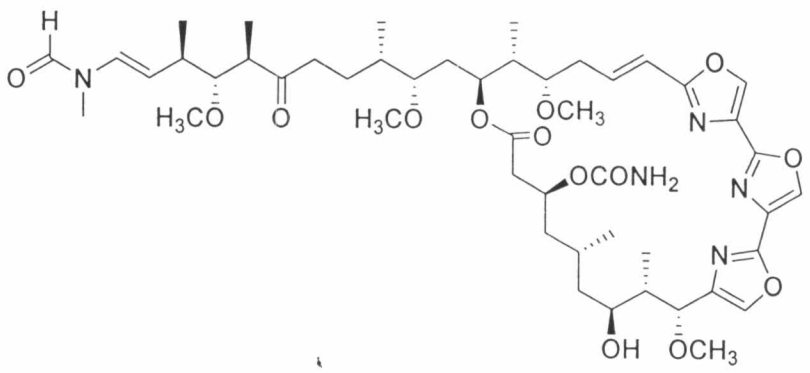

Figure 16 The structure of kabiramide C.

Table 8 The ^{1}H, ^{13}C NMR, and ^{1}H-^{13}C long-range correlations in HMBC ($^{n}J_{CH}$ = 8 Hz) spectral data in $CDCl_3$ of kabiramide C.

Position	Kabiramide C (Matsunaga et al., 1986)		Kabiramide C (isolated)		HMBC correlations ($^{n}J_{CH}$ = 8 Hz, n=2, 3)
	δ_H	δ_C	δ_H (ppm), mult. (*J* in Hz)	δ_C	
1	-	171.6	-	171.21	
2	2.39, 2.56	43.0	2.38, 2.57, 1H each	42.83	C-1
3	5.13	69.3	5.30, 1H, m	69.13	
3-$OCONH_2$	6.48	157.3	-	156.96	
4	1.31, 1.82	45.1	1.28, 1.83, 1H each	44.76	
5	1.89	25.1	1.88, 1H	24.99	
5-CH_3	0.89	18.2	0.92, 3H, d (6.5)	18.40	C-5
6	1.66, 1.66	43.6	1.64, 2H	43.55	
7	3.81	74.4	3.82, 1H, m	73.08	
7-OH	3.13	-	-	-	
8	2.13	37.3	2.13, 1H, m	37.38	
8-CH_3	0.97	10.6	0.98, 3H, d (6.7)	10.88	C-8, C-9
9	4.78	78.3	4.79, 1H, br s	78.24	8-CH_3, C-10
9-OCH_3	3.42	57.6	3.44, 3H, s	57.52	C-9
10	-	141.6	-	141.03	
11	7.55	135.5	7.57, 1H, d (0.5)	135.44	C-10, C-12
12	-	155.4	-	155.07	
13	-	131.1	-	130.80	
14	8.07	136.8	8.09, 1H, s	136.71	C-13, C-15
15	-	156.4	-	156.06	
16	-	129.9	-	129.59	
17	8.01	137.1	8.03, 1H, s	137.02	C-16, C-18
18	-	163.2	-	162.78	
19	6.26	115.4	6.28, 1H, d (15.9)	115.28	
20	7.44	142.0	7.45, 1H, ddd (15.9, 9.7, 5.9)	141.62	
21	2.38, 2.78	34.0	2.35, 2.76, 1H each	33.88	
22	3.65	79.2	3.65, 1H, m	79.03	
22-OCH_3	3.40	57.4	3.42, 3H, s	57.37	C-22
23	1.82	40.5	1.80, 1H	40.41	
23-CH_3	0.85	8.4	0.86, 3H, d (6.9)	8.52	C-22, C-23, C-24

Table 8 (continued)

Position	Kabiramide C (Matsunaga et al., 1986)		Kabiramide C (isolated)		HMBC correlations ($^nJ_{CH}$ = 8 Hz, n=2, 3)
	δ_H	δ_C	δ_H (ppm), mult. (*J* in Hz)	δ_C	
24	5.29	74.1	5.14, 1H, m	73.84	
25	1.44, 1.63	33.1	1.41, 1.69, 1H each	32.86	
26	2.99	82.0	2.98, 1H	81.86	
26-OCH_3	3.30	57.9	3.31, 3H, s	57.76	C-26
27	1.69	34.6 [34.7]	1.77, 1H	34.49	
27-CH_3	0.80	15.5	0.81, 3H, d (6.6)	15.56	C-26, C-27, C-28
28	1.25, 1.75	25.1 [25.0]	1.26, 1.77, 1H each	24.89	
29	2.49, 2.49	42.3 [42.4]	2.47, 2H	42.33 [42.26]	
30	-	214 [214.1]	-	213.70 [213.79]	
31	2.66 [2.63]	49.0 [49.1]	2.64	48.89 [49.07]	C-28
31-CH_3	0.87	13.5 [13.6]	0.90, 3H, d (6.9)	13.58	C-30, C-31, C-32
32	3.28	87.3 [87.4]	3.24, 1H	87.14 [87.22]	
32-OCH_3	3.31	61.3	3.33, 3H, s	61.24	C-32
33	2.40	37.4 [37.6]	2.38, 1H	37.52 [37.58]	
33-CH_3	1.13	19.3 [19.4]	1.14. 3H, d (7.2)	19.36	C-32, C-33, C-34
34	5.08 [5.10]	111.4 [113.2]	5.09, 1H, m	111.16 [112.93]	
35	6.43 [7.10]	128.7 [124.8]	6.45 [7.11], 1H, d (14.6)	128.49 [124.48]	C-33, 35-NCH_3
35-NCH_3	3.00 [3.05]	27.6 [33.1]	3.02 [3.06], 1H, s	27.59 [33.10]	C-35, 35-NCHO
35-NCHO	8.26 [8.04]	162.1 [160.8]	8.27 [8.06], 1H, s	161.86 [160.59]	35-NCH_3

Chemical shifts for minor conformer are in brackets.

1.2 Identification of kabiramide D

Kabiramide D was obtained as a white amorphous solid. The UV and IR spectra (Figures 49-50) of kabiramide D were similar to those of kabiramide C. This compound showed UV absorption of three consecutive oxazole rings conjugating with a double bond at λ_{max} 245 nm. The IR spectrum (Figure 50) indicated the presence of hydroxyl (3443 cm^{-1}), ketone (1728 cm^{-1}), ester (1691 cm^{-1}), and amide (1656 cm^{-1}) moieties. This compound showed specific rotation $[\alpha]^{23}_{D}$ -13.51 ° (*c* 0.094, MeOH).

The ^{1}H NMR spectrum revealed that kabiramide D has the same skeleton as kabiramide C. In the ^{1}H NMR spectrum (Figure 51) of kabiramide D, double proton signals due to the two geometric forms were observed in the ratio of 2:1 for the formamide protons (δ 8.24 and 8.03 ppm), *N*-methyl protons (δ 2.99 and 3.03 ppm), and H-35 (δ 6.41 and 7.07 ppm). The trisoxazole moiety was characterized by three singlet proton signals at δ 8.10 (H-14), 8.05 (H-17), and 7.63 (H-11) ppm. The ^{1}H NMR spectrum also showed the signals of six methyl protons [δ 1.10, 0.96, 0.89, 0.84, and 0.75 (6H) ppm], four methoxy protons (δ 3.36, 3.28, 3.26, and 3.25 ppm), and two olefinic protons (δ 7.03 and 6.24 ppm).

The ^{13}C NMR spectrum (Figure 52) of kabiramide D was also similar to those of kabiramide C. The ^{13}C NMR spectrum showed forty-seven carbons which could be classified by DEPT 90 and DEPT 135 spectra (Figures 53-54) as eleven methyl carbons, seven methylene carbons, twenty-one methine carbons, and eight quaternary carbons. The duplication of some carbon signals was presented due to the restricted rotation around the C–N bond of *N*-methyl formamide group as in kabiramide C.

The H,H COSY and HMQC spectra (Figures 54-55) revealed the partial structures of C-2 to C-11, C-19 to C-22, 23-CH_3 to 27-CH_3, C-28 to C-32, and 33-CH_3 to C-35 (Figure 17) which werealso found in kabiramide C. The connectivity of these fragments was achieved by analysis of HMBC spectrum ($^{n}J_{HC}$ = 8 Hz, Figures 56-57). Additionally, the HMBC spectrum also showed the correlation between proton and carbon in each oxazole ring (Figure 17).

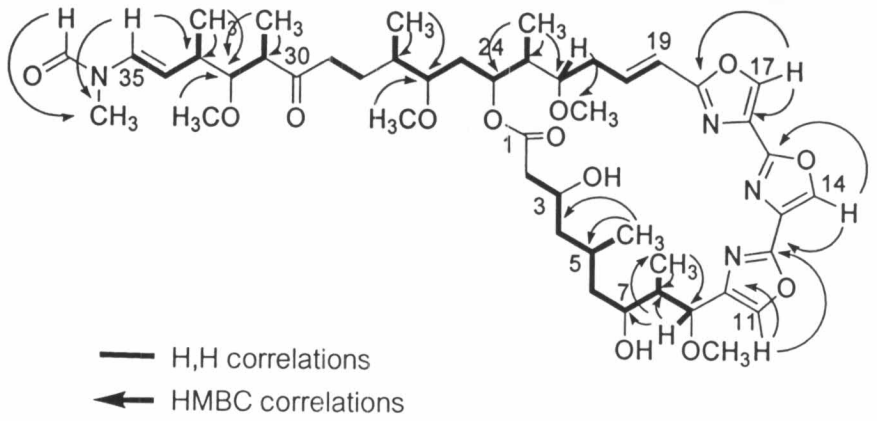

Figure 17 The H,H correlations (bold line) and HMBC correlations (arrow) of kabiramide D.

Furthermore, the ESI mass spectrum (Figure 48) of kabiramide D presented the pseudomolecular ion peak at *m/z* 921.4836 $[M+Na]^+$, implying the molecular formula $C_{47}H_{70}N_4O_{13}$, that was 43 mass unit less than kabiramide C. In addition, the upfield shift of H-3 in kabiramide D (δ 4.24 ppm) compared with that of kabiramide C (δ 5.30 ppm) and the disappearance of carbonyl signal at δ 156.93 ppm in kabiramide D suggested the absence of the carbamoyl moiety at C-3. These spectral data as well as comparison with literature (Table 9; Matsunaga et al., 1989; Klenchin et al. 2003; Tanaka et al., 2003) led to assign this compound as kabiramide D, the 3-decarbamoyl derivative of kabiramide C, which was previously isolated from nudibranch *Hexabranchus* sp. egg masses (Matsunaga et al., 1989).

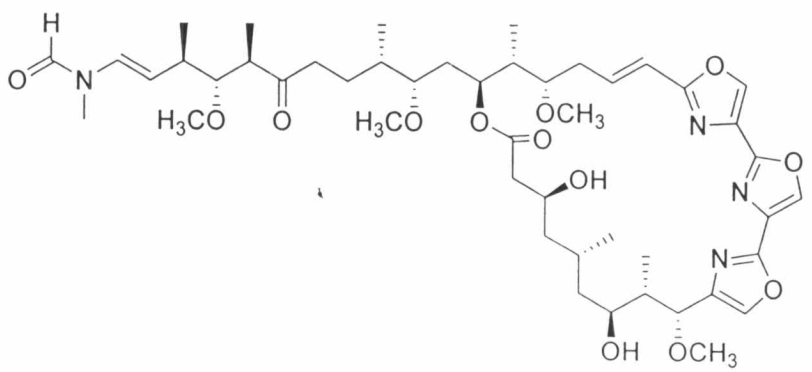

Figure 18 The structure of kabiramide D.

Table 9 The ^{1}H, ^{13}C NMR, and ^{1}H-^{13}C long-range correlations in HMBC ($^{n}J_{CH}$ = 8 Hz) spectral data in $CDCl_3$ of kabiramide D.

Position	Kabiramide D (Matsunaga et al., 1989)		Kabiramide D (isolated)		
	δ_H	δ_C	δ_H (ppm), mult. (*J* in Hz)	δ_C	HMBC correlations ($^{n}J_{CH}$ = 8 Hz, n=2, 3)
1	-	172.7	-	172.35	
2	2.32, 2.45	43.9[a]	2.43, 2.29, 1H each	43.68	C-1
3	4.27	67.1[b]	4.24, 1H, t (10.5)	67.01	
3-OH	-	-	-	-	
4	0.99, 1.91	44.7[a]	0.93, 1.89, 1H each	44.75	
5	2.25	24.9	2.22, 2H	24.73	
5-CH_3	0.99	21.1	0.96, 3H, d (6.4)	21.08	C-4, C-5
6	1.47, 1.52	44.4[a]	1.46, 1.53, 1H each	44.44	
7	3.84	71.3[b]	3.80, 1H, m	71.10	
7-OH	-	-	-	-	
8	2.20	40.2[c]	2.18, 1H	42.48	
8-CH_3	0.80	13.5	0.75, 3H, d (6.9)	13.67	C-8, C-9
9	4.41	78.8	4.36, 1H, d (2.1)	79.70	C-7, C-8, 8-CH_3, 9-OCH_3
9-OCH_3	3.38	58.1	3.36, 3H, s	57.64	C-9
10	-	139.6	-	139.11	
11	7.63	137.2	7.63, 1H, s	137.09	C-10, C-12
12	-	155.5	-	155.23	
13	-	131.1	-	130.73	
14	8.10	137.3	8.10, 1H, s	137.09	C-13, C-15
15	-	156.8	-	156.39	
16	-	130.0	-	129.66	
17	8.06	137.5	8.05, 1H, s	137.31	C-16, C-18
18	-	163.0	-	162.64	
19	6.27	116.4	6.24, 1H, d (15.8)	116.06	
20	7.08	141.3	7.03, 1H, ddd (15.8, 10.7, 4.7)	141.16	
21	2.32, 2.71	34.0	2.30, 2.68, 1H each	34.02	
22	3.50	79.9	3.48, 1H, d (8.7)	78.45	22-OCH_3
22-OCH_3	3.29	57.7	3.25, 3H, s	57.23	C-22
23	1.62	42.5[c]	1.58, 1H	40.08	
23-CH_3	0.87	9.1	0.84, 3H, d (7.6)	9.10	C-22, C-23, C-24

Table 9 (continued)

Position	Kabiramide D (Matsunaga et al., 1986)		Kabiramide D (isolated)		
	δ_H	δ_C	δ_H (ppm), mult. (*J* in Hz)	δ_C	HMBC correlations ($^nJ_{CH}$ = 8 Hz, n=2, 3)
24	5.27	72.5[b]	5.24, 1H, t (9.4)	72.33	
25	1.40, 1.60	33.2	1.35, 1.57, 1H each	33.18	
26	2.89	81.9	2.85, 1H, d (8.8)	81.74	
26-OCH_3	3.30	58.1	3.26, 3H, s	57.95	C-26
27	1.70	34.7	1.64	34.02 [34.60]	
27-CH_3	0.78	15.6	0.75, 3H, d (5.172)	15.65	C-26, C-27
28	1.23, 1.75	25.0	1.25, 1.70, 1H each	24.96 [25.05]	
29	2.49, 2.49	42.5	2.45, 2H	42.37 [42.29]	
30	-	214.1 [214.2]	-	213.72 [213.86]	
31	2.65 [2.62]	49.1	2.63, 1H	49.07 [49.15]	
31-CH_3	0.90	13.7	0.89, 3H, d (9.4)	13.67	C31, C-32
32	3.27	87.4 [87.5]	3.25, 1H	87.23 [87.33]	
32-OCH_3	3.31	61.4	3.28, 3H, s	61.32	C-32
33	2.37	37.5 [37.7]	2.35, 1H	37.48 [37.68]	
33-CH_3	1.13	19.4	1.10, 3H, d (6.8)	19.43	C-32, C-33, C-34
34	5.08 [5.09]	111.5 [113.2]	5.06, 1H, m	111.25 [113.00]	
35	6.42 [7.10]	128.8 [124.8]	6.41 [7.07], 1H, d (14.4)	128.56 [124.57]	C-33, C-34, 35-NCH_3
35-NCH_3	3.01 [3.05]	27.7 [33.2]	2.99 [3.03], 1H, s	27.69 [33.18]	C-35, 35-NCHO
35-NCHO	8.26 [8.05]	162.2 [160.9]	8.24 [8.03], 3H, s	161.92 [160.64]	35-NCH_3

Chemical shifts for minor conformer are in brackets.

[a-c]Assignments may be interchanged within column.

1.3 Identification of kabiramide F

Kabiramide F, the most polar compound of the three isolated kabiramides, was obtained as a white amorphous solid. This compound has molecular formula $C_{46}H_{68}N_4O_{13}$ as deduced by ESI mass spectrum (Figure 58), *m/z* 907.4679 $[M+Na]^+$. This compound has 57 (C_2H_3NO) and 14 (CH_2) mass units less than kabiramides C and D, respectively. The UV and IR spectra (Figures 59-60) of kabiramide F were identical to those of kabiramides C and D. The UV spectrum exhibited the absorption at λ_{max} 245 nm indicating the common character of three consecutive oxazole rings conjugating with a double bond. The IR spectrum (Figure 60) showed the absorption band of hydroxyl (3419 cm^{-1}), ketone (1713 cm^{-1}), ester (1693 cm^{-1}), and amide (1655 cm^{-1}) groups. This compound showed the specific rotation $[\alpha]^{23}_{D}$ –14.99° (*c* 0.085, MeOH).

The ^1H and ^{13}C NMR spectra (Figures 62 and 64) of kabiramide F in $CDCl_3$ can almost be superimposed on those of kabiramides C and D. Attemps to perform the 2D NMR experiments in $CDCl_3$ solution failed due to the decomposition of the compound during the experiment. Therefore, the NMR experiments were mainly obtained in DMSO-d_6 solution.

In the ^1H NMR spectrum (in DMSO-d_6, Figure 61), the trisoxazole moiety was characterized by three singlet proton signals at δ 8.87 (H-14), 8.81 (H-17), and 8.08 (H-11) ppm. The double proton signals, due to the two geometric forms of *N*-formyl group, were observed in the ratio of 2:1 for the *trans* coupled olefinic protons, H-34 (δ 4.98 and 5.06 ppm) and H-35 (δ 6.75 and 6.99 ppm), 35-NCHO (δ 8.34 and 8.08 ppm), and 35-NCH_3 (δ 2.88 and 3.00 ppm). The ^1H NMR also presented another couple of the *trans*-olefinic protons at δ 6.45 (H-19) and 6.95 (H-20) ppm.

The analysis of H,H COSY spectrum (in DMSO-d_6, Figure 67) revealed the consecutive proton connectivity as follows: H_a-2/H_b-2/H-3/3-OH/H_a-4/H_b-4/H-5/ 5-CH_3/H_a-6/H_b-6/H-7/7-OH/H-8/8-CH_3/H-9/H-11, H-19/H-20/H-21/H-22/22-OH, 23-CH_3/

H-23/H-24/H_a-25/H_b-25/H-26/H-27/27-CH_3, H_a-28/H_b-28/H-29, and CH_3-31/H-31/H-32/H-33/33-CH_3/H-34/H-35 (Figure 19).

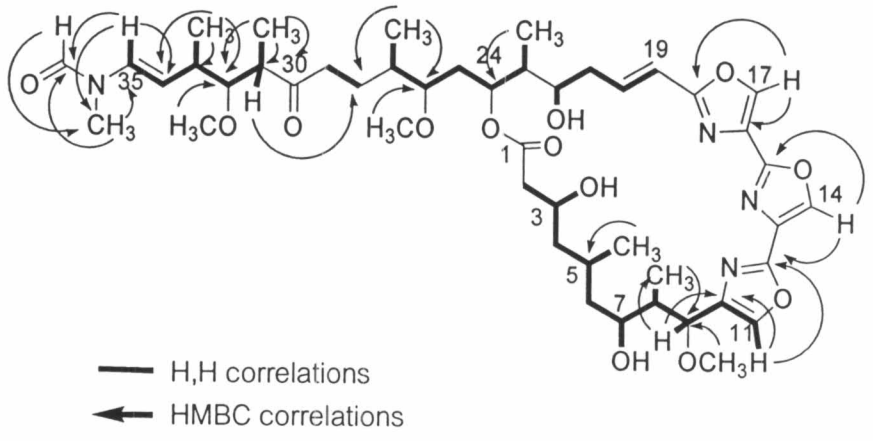

Figure 19 The H,H correlations (bold line) and HMBC correlations (arrow) of kabiramide F.

The ^{13}C NMR spectrum of kabiramide F in DMSO-d_6 (Figure 63) was similar to its spectrum in $CDCl_3$. The double carbon signals in the ratio 2:1 due to its two geometric forms were also observed for C-33 (δ 36.68 and 36.82 ppm), C-34 (δ 110.02 and 112.52 ppm), C-35 (δ 129.34 and 124.17 ppm), 35-NCHO (δ 162.42 and 161.16 ppm), and 35-NCH_3 (δ 26.85 and 32.66 ppm). Comparison of the ^1H and ^{13}C NMR spectral data of kabiramide F with those of kabiramide C suggested that one methoxy group was missing. The ^{13}C NMR also revealed the absence of carbamoyl ester at C-3. These data, together with the presence of two additional hydroxyl groups in ^1H NMR spectrum, indicated that a methoxy group and the carbamoyl group of kabiramide C were replaced with hydroxyl groups.

The HMQC spectrum (Figure 66) indicated the one-bond connection of protons and carbons as shown in Table 10. Interpretation of HMBC ($^nJ_{HC}$ = 8 Hz, in DMSO-d_6, Figures 68-69) established the connection of each fragment and the position of methoxy groups and carbons in each oxazole ring (Figure 19). The HMBC spectral data did not show the correlation from any methoxy groups to C-22, so it was confirmed that the methoxy group at C-22 in kabiramide C was substituted by hydroxy group in

kabiramide F. The chemical shift of H-24 at δ 5.07 ppm suggested that the ester group was attached at C-24.

Assignments of absolute configuration of the chiral carbons were proposed by comparison to previous reports of kabiramide C (Matsunaga et al., 1989; Klenchin et al. 2003; Tanaka et al., 2003) and the structure is shown in Figure 20. Therefore, kabiramide F is the 22-demethyl derivative of kabiramide D, a new member of the kabiramide class.

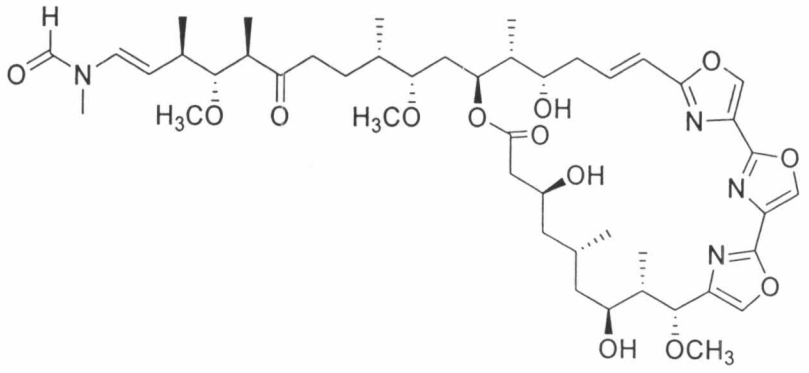

Figure 20 The structure of kabiramide F.

Table 10 The ^{1}H, ^{13}C NMR, and ^{1}H-^{13}C long-range correlations in HMBC ($^{n}J_{CH}$ = 8 Hz) spectral data in DMSO-d_6 and $CDCl_3$ of kabiramide F.

Position	Kabiramide F (in DMSO-d_6)			Kabiramide F (in $CDCl_3$)	
	δ_H (ppm), mult. (*J* in Hz)	δ_C	HMBC correlations ($^{n}J_{CH}$ = 8 Hz, n=2, 3)	δ_H (ppm), mult. (*J* in Hz)	δ_C
1	-	171.32		-	173.62
2	2.45, 2.34, 1H each	43.46		2.50, 2.37, 1H each	44.36
3	4.01, 1H, br s	65.28		4.29, 1H, t (10.0)	67.08
3-OH	4.52, 1H, d (6.1)	-		-	-
4	1.76, 1.02, 1H each	43.88		1.89, 1.07, 1H each	44.73
5	1.93, 1H	25.44		2.11, 1H	25.52
5-CH_3	0.85, 3H, d (5.7)	20.63	C-5	0.95, 3H, d (6.6)	20.02
6	1.38, 1.25, 1H each	41.70		1.64, 1.56, 1H each	43.96
7	3.79, 1H	69.13		3.85, 1H	72.09
7-OH	4.28, 1H, d (3.8)	-		-	-
8	2.04, 1H	43.27		2.13, 1H	41.22
8-CH_3	0.75, 3H, d (6.6)	11.52		0.87, 3H, d (7.0)	12.89
9	4.33, 1H, d (4.7)	78.33	C-10	4.49, 1H	79.13
9-OCH_3	3.19, 3H, s	57.03	C-9	3.33, 3H, s	57.48
10	-	141.05		-	139.93
11	8.08, 1H, s	136.87	C-10, C-12	7.62, 1H, s	136.63
12	-	154.29		-	155.28
13	-	130.38		-	130.57
14	8.87, 1H, s	139.23	C-13, C-15	8.10, 1H, s	137.29
15	-	155.47		-	156.30
16	-	129.34		-	129.45
17	8.81, 1H, s	139.23	C-16, C-18	8.03, 1H, s	137.01
18	-	161.78		-	163.13
19	6.45, 1H, d (15.5)	116.19		6.26, 1H, d (15.9)	115.28
20	6.95, 1H, dt (15.5, 7.6)	140.27		7.09, 1H, m	143.16
21	2.41, 2.41, 1H each	38.77		2.57, 2.37, 1H each	38.00
22	3.72, 1H, br s	68.87		4.05, 1H	68.52
22-OH	4.55, 1H, d (4.9)	-		-	-
23	1.67, 1H	40.30		1.60, 1H	42.00
23-CH_3	0.83, 3H	8.79		0.89, 3H, d (6.5)	9.10

Table 10 (continued)

Position	Kabiramide F (in DMSO-d_6)			Kabiramide F (in $CDCl_3$)	
	δ_H (ppm), mult. (*J* in Hz)	δ_C	HMBC correlations ($^nJ_{CH}$ = 8 Hz, n=2, 3)	δ_H (ppm), mult. (*J* in Hz)	δ_C
24	5.07, 1H	72.86		5.08, 1H	73.51
25	1.58, 1.40, 1H each	32.28		1.67, 1.44, 1H each	33.76
26	2.95, 1H	80.66		2.98, 1H	81.94
26-OCH_3	3.28, 3H, s	57.57	C-26	3.28, 3H, s	58.08
27	1.65, 1H	33.94		1.70, 1H	34.69
27-CH_3	0.75, 3H, d (6.6)	15.31	C-26, C-27	0.80, 3H, d (6.8)	15.63
28	1.63, 1.13, 1H each	24.63		1.72, 1.26, 1H each	25.06
29	2.48, 2.48, 1H each	40.84		2.50, 2.50, 1H each	42.37
30	-	213.01		-	213.66
31	2.62, 1H	48.45	C-28	2.67, 1H	49.13
31-CH_3	0.85, 3H, d (5.7)	13.32	C-30, C-31, C-32	0.91, 3H, d (6.5)	13.70
32	3.20, 1H	86.32		3.27, 1H	87.32 [87.42]
32-OCH_3	3.21, 3H, s	60.26		3.31, 3H, s	61.35
33	2.41, 1H	36.68 [36.82]		2.40, 1H	37.53 [37.73]
33-CH_3	1.50, 3H, d (6.7)	18.92	C-32, C-33, C-34	1.12, 3H, d (6.7)	19.46
34	4.98 [5.06], 1H	110.02 [112.52]		5.08, 1H	113.07 [111.33]
35	6.75 [6.99] , 1H, d (14.1)	129.34 [124.17]	C-33, 35-NCH_3	6.43 [7.09] , 1H, d (14.1)	128.62 [124.65]
35-NCH_3	2.88 [3.00] , 3H, s	26.85 [32.66]	C-35, 35-NCHO	3.00 [3.04] , 3H, s	27.74 [33.20]
35-NCHO	8.34 [8.08] , 1H, s	162.42 [161.16]	35-NCH_3	8.25 [8.06] , 1H	161.94 [160.66]

Chemical shifts for minor conformer are in brackets.

2. Synthesis of the 7-(4-aminomethyl-1*H*-1,2,3-triazol-1-yl)kabiramide C

Recently, some literatures reported that kabiramide C was an actin-targeted trisoxazole macrolide and functioned as unregulated biomimetics of actin filament barbed end capping protein (Klenchin et al., 2003; Tanaka et al., 2003). These studies suggested that optical and chemical probes based on kabiramide C could provide new information on the regulation of actin filament dynamics in living cells. Analysis of the high resolution structure of the kabiramide C-G-actin complex revealed that optical probes linked to the 7-hydroxy group of kabiramide C would be a suitable site because it does not engage in direct contact with actin and should therefore not interfere with actin-binding. For the approach to the design and synthesis of functional optical probes of kabiramide C, we elected to introduce an amino-group to the 7-position since this would allow a facile route for the preparation of kabiramide C probes using commercially available succinimidyl esters.

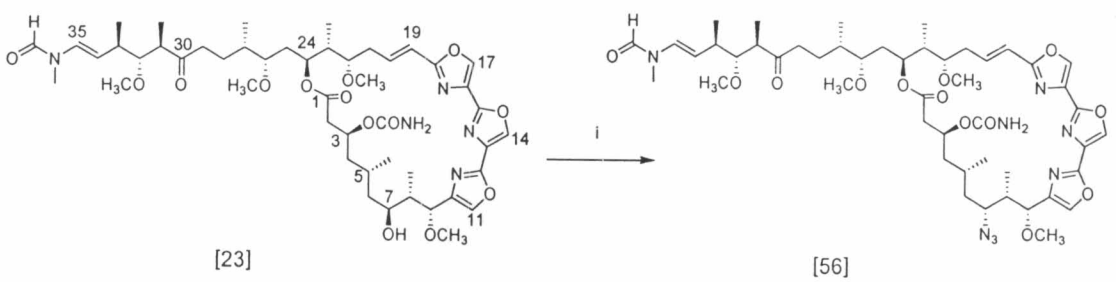

[23] [56]

Figure 21 Synthesis of 7-azidokabiramide C: (i) HN_3, PPh_3, DIAD, dry THF, rt, 40.5%.

In the first step, kabiramide C was converted to 7-azidokabiramide C **[56]** *via* the Mitsunobu reaction (Mitsunobu, 1981; Stachel et al., 2000; Ko, 2002) by using hydrazoic acid as a nucleophile in the presence of triphenylphosphine (PPh_3) and diisopropyl azodicarboxylate (DIAD; Figure 21). The reaction was performed at room temperature under nitrogen atmosphere for 4 hours to give 7-azidokabiramide C (40.5% yield). This reaction underwent the S_N2 mechanism as proposed in Figure 22.

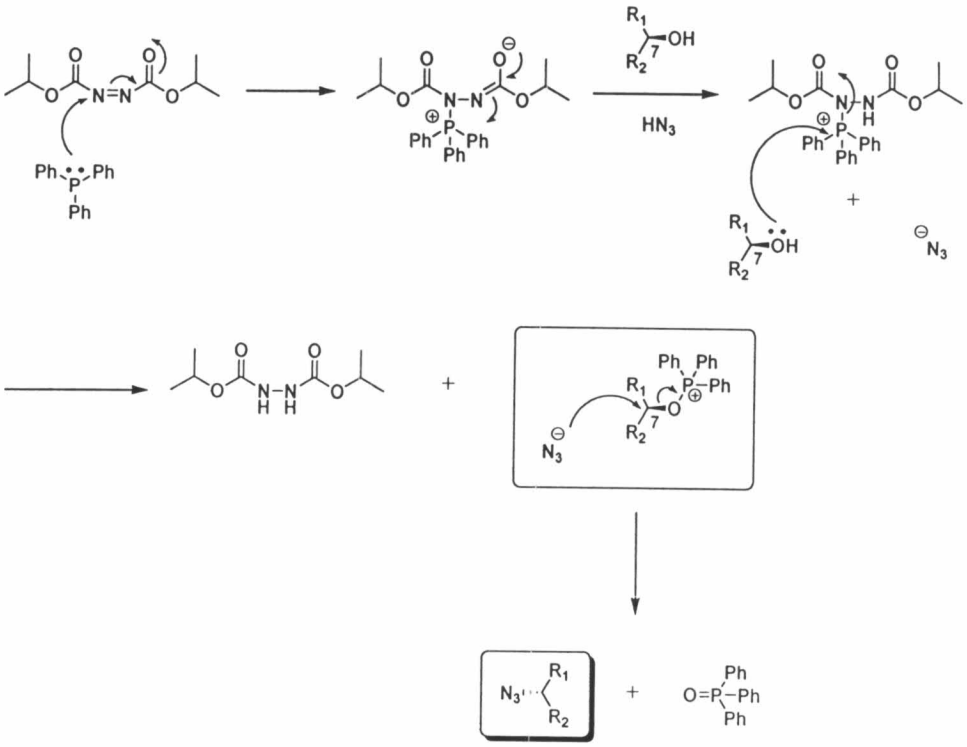

Figure 22 Proposed mechanism of Mitsunobu reaction (Mitsunobu, 1981).

Comparison of the ^{1}H NMR spectral data of 7-azidokabiramide C (Figure 73) with those of kabiramide C showed that the proton signal at C-7 was shifted upfield to 3.52-3.44 ppm. Additionally, the ESI mass spectrum (Figure 70) confirmed the molecular formula of $C_{48}H_{70}N_8O_{13}$ by showing the pseudomolecular ion peak at *m/z* 989.4691 $[M+Na]^+$. The physical properties, including UV absorption (Figure 71), IR absorption (Figure 72) and specific rotation, ^{1}H and ^{13}C NMR (Figures 73-74) spectral data of this compound are shown in Tables 12-14.

7-Azidokabiramide C was then coupled to 3-aminopropyne using 1,3-dipolar cycloaddition reaction to create the 1,2,3-triazole lingkage (Horne et al., 2003). First, the amino group of 3-aminopropyne was protected as 3-(fluoren-9-yl-methoxycarbonyl) aminopropyne **[59]** by using *N*-(9*H*-fluoren-9-yl-methoxycarbonyloxy) succinimide (FmocNHS) as shown in Figure 23. The percentage yield for the preparation of 3-(fluoren-9-yl-methoxycarbonyl)aminopropyne was 73.7%. The ESI mass spectrum (Figure 75) of **[59]** showed the molecular ion peak at m/z 277.1114 $[M]^+$

molecular formula of $C_{18}H_{15}NO_2$. This compound exhibited the UV absorption (in MeOH, Figure 76) at λ_{max} 266, 290, and 300 nm. The IR spectrum (Figure 77) showed absorption band at 3453, 3307, 3066-2954, 1725, and 1510 CM^{-1}. The analysis of ^{1}H and ^{13}C NMR spectral data (Figures 78-79) are shown in the Table 11.

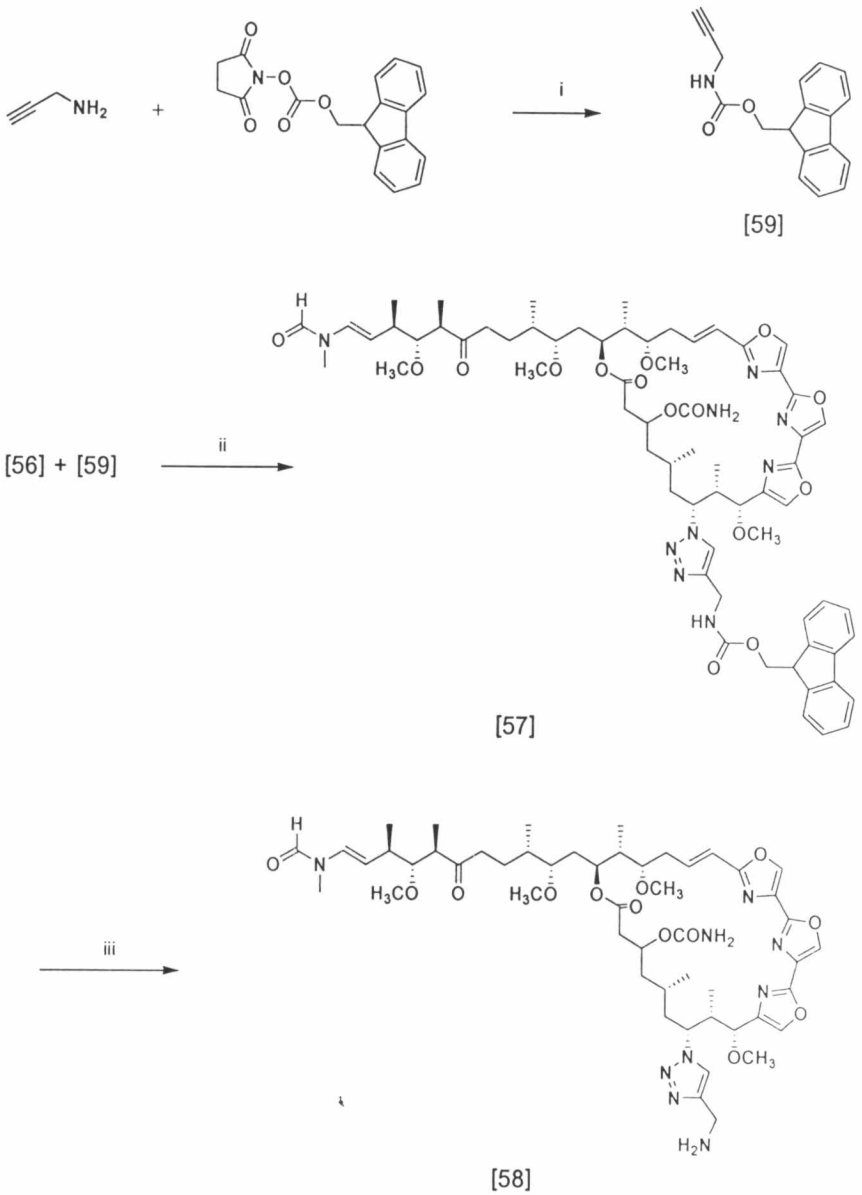

Figure 23 Synthesis of 7-(4-aminomethyl-1*H*-1,2,3-triazol-1-yl)kabiramide C [58]: (i) THF, 0 $^{o}C \longrightarrow$ rt, 73.7 %; (ii) MeOH/H_2O, Et_3N, CuI, rt, 63.4 %; (iii) 20% v/v piperidine in dry CH_2Cl_2, rt, 30.8 %.

Table 11 The ^{1}H and ^{13}C NMR spectral data in $CDCl_3$ of 3-(fluoren-9-yl-methoxy-carbonyl)aminopropyne.

Position	3-(fluoren-9-yl-methoxy-carbonyl)aminopropyne	
	δ_H (ppm), mult. (*J* in Hz)	δ_C (ppm)
1	2.62,1H, t (2.6)	71.62
2	-	79.59
3	4.01, 2H, dd (5.4, 2.2)	30.75
Fmoc 1	7.59, 1H, d (7.4)	127.66
Fmoc 2	7.32, 1H, dt (7.5, 1.3)	124.95
Fmoc 3	7.41, 1H, dt (7.6, 0.8)	119.93
Fmoc 4	7.77, 1H, d (7.2)	126.99
Fmoc 4a	-	141.22
Fmoc 4b	-	141.22
Fmoc 5	7.77, 1H, d (7.2)	126.99
Fmoc 6	7.41, 1H, dt (7.6, 0.8)	119.93
Fmoc 7	7.32, 1H, dt (7.5, 1.3)	124.95
Fmoc 8	7.59, 1H, d (7.4)	127.66
Fmoc 8a	-	143.70
Fmoc 9	4.23, 1H, t (6.5)	47.03
Fmoc 9a	-	143.70
Fmoc CO	-	155.86
Fmoc CH_2	4.44, 2H, d (6.7)	66.97

The 7-azidokabiramide C **[56]** was reacted with 3-(fluoren-9-yl-methoxycarbonyl)aminopropyne **[59]** in the presence of catalytic amount of copper iodide (CuI) and triethylamine (Et_3N) to afford 7-[4-*N*-(9*H*-fluoren-9-yl-methoxycarbonyl) aminomethyl-1,2,3-triazol-1-yl]kabiramide C **[57]** in 63.4% yield (Figure 32). The presence of Cu(I) salt in 1,3-dipolar cycloaddition reaction of terminal alkyne with azide not only catalyzed the reaction but also improved the regioselectivity to give the 1,4-substituted 1,2,3-triazole (Rostovsev et al., 2002; Tornøe et al., 2002; Wang and Qin, 2003). The proposed mechanism is shown in Figure 24.

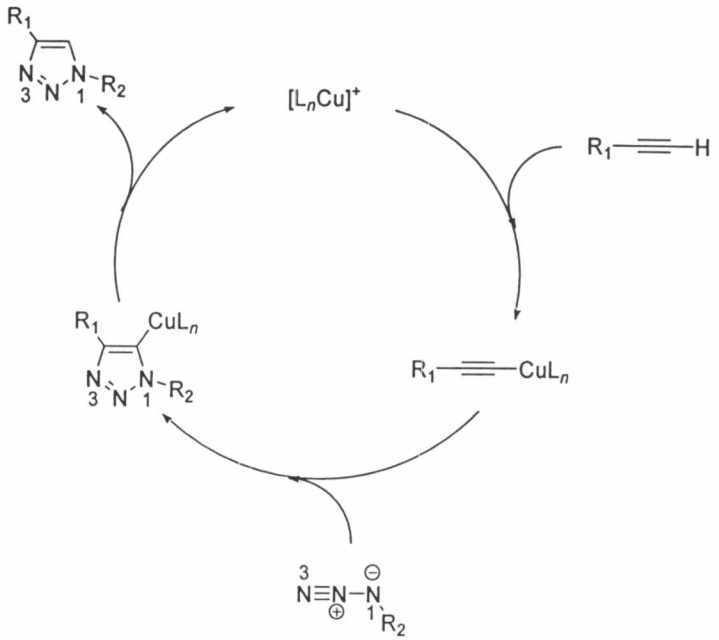

Figure 24 Proposed mechanism of regioselective 1,4-substituted 1,3-dipolar cycloaddition (Breinbauer and Köhn, 2003).

The structure of **[57]** was confirmed by the presence of proton signals of Fmoc i.e. eight aromatic proton signals at δ 7.76 (2H), 7.58 (2H), 7.40 (2H), and 7.30 (2H) ppm, one methylene proton signal at δ 4.40 (2H) ppm, and one methine proton signal at δ 4.22 ppm in the ^{1}H NMR spectrum (Figure 83). In addition, the ESI mass spectrum (Figure 80) exhibited the pseudomolecular ion peak at *m/z* 1266.6033 $[M+Na]^{+}$ indicating the molecular formula of $C_{66}H_{85}N_9O_{15}$. The physical properties, including UV absorption (Figure 81), IR absorption (Figure 82), specific rotation, ^{1}H and ^{13}C NMR (Figures 83-84) spectral data of this compound are shown in Tables 12-14.

Finally, deprotection of Fmoc with 20% piperidine in dry CH_2Cl_2 at room temperature gave 7-(4-aminomethyl-1*H*-1,2,3-triazol-1-yl)kabiramide C (AMT-KabC) **[58]** (Figure 23) in 30.8% yield. The mechanism of action is shown in Figure 25. The ^{1}H NMR spectrum (Figure 88) clearly showed that the proton signals of Fmoc were absent. Comparison of the ^{1}H NMR spectral data of AMT-KabC with those of kabiramide C

revealed a triazole proton signal at δ 7.49 ppm and an amino methylene proton signal at δ 4.01 ppm. Furthermore, the methoxy proton signal at C-9 was shifted upfield from δ 3.44 ppm (kabiramide C) to δ 3.15 ppm (AMT-KabC) because of the electron shielding effect of the triazole ring. The ESI mass spectrum (Figure 85) gave the pseudomolecular ion peak at *m/z* 1022.5574 $[M+H]^+$ supporting the molecular formula of $C_{51}H_{75}N_9O_{13}$. The UV (Figure 86), IR (Figure 87), specific rotation, ^{1}H NMR (Figure 88), and ^{13}C NMR (Figure 89) spectral data of this compound are shown in Tables 12-14.

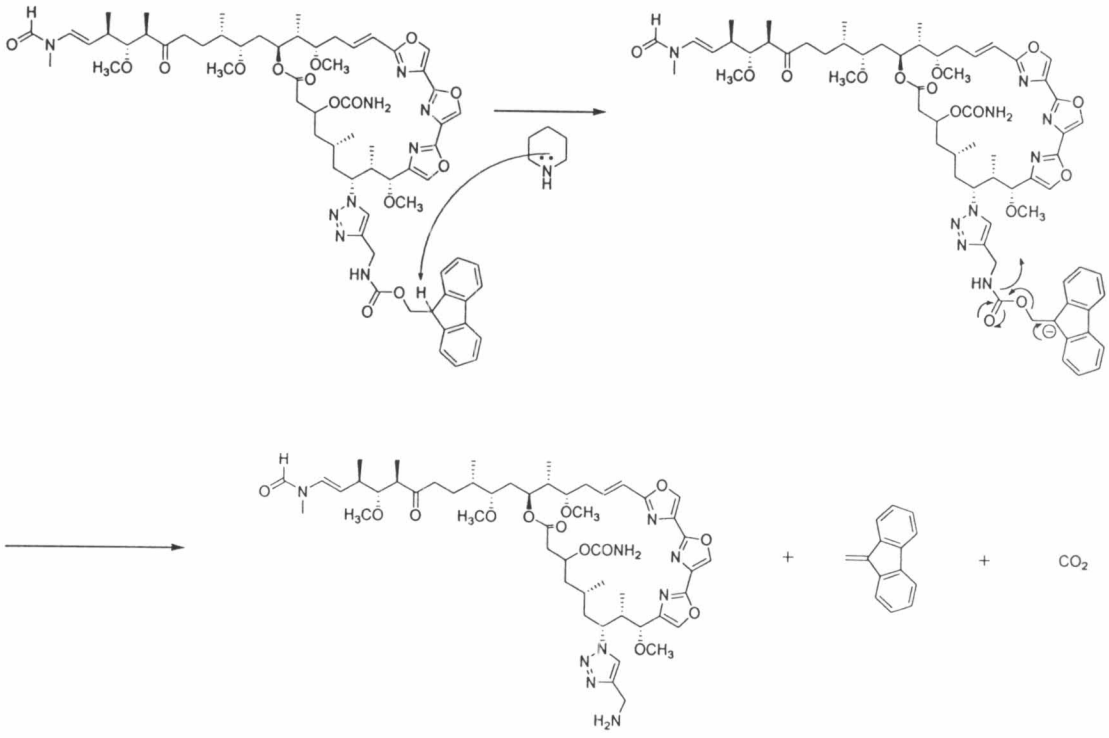

Figure 25 Proposed mechanism of the deprotection of 7-[4-*N*-(9*H*-fluoren-9-yl-methoxycarbonyl)aminomethyl-1,2,3-triazol-1-yl]kabiramide C.

Table 12 The UV, IR, and specific rotation of 7-azidokabiramide C **[56]**, 7-[4-*N*-(9*H*-fluoren-9-yl-methoxycarbonyl)aminomethyl-1,2,3-triazol-1-yl]kabiramide C **[57]**, and 7-(4-aminomethyl-1*H*-1,2,3-triazol-1-yl)kabiramide C **[58]**.

Compound	UV (MeOH) λmax (log ε) nm	IR ($CHCl_3$, cm^{-1})	$[\alpha]^{23}_D$ ($CHCl_3$)
[56]	247 (4.12)	3464, 3347, 3166, 3020-2935, 2104, 1720, 1657	- 6.27 ° (*c* 0.047)
[57]	255 (4.49), 299 (3.82)	3453, 3348, 3072, 3006-2883, 1721, 1655, 1513	+ 3.06 ° (*c* 0.032)
[58]	246 (4.12)	3464, 3352, 3072-2884, 1722, 1655	- 3.87 ° (*c* 0.012)

Table 13 The ^{1}H NMR spectral data of 7-azidokabiramide C **[56]**, 7-[4-*N*-(9*H*-fluoren-9-yl-methoxycarbonyl)aminomethyl-1,2,3-triazol-1-yl]kabiramide C **[57]**, and 7-(4-aminomethyl-1*H*-1,2,3-triazol-1-yl)kabiramide C **[58]**.

Position	δ_H (ppm), mult. (*J* in Hz)		
	[56]	[57]	[58]
1	-	-	-
2	2.90-1.20	2.83-1.20	2.83-1.20
3	5.31, 1H, m	5.31, 1H, m	5.30, 1H, m
3-OH	-	-	-
4	2.90-1.20	2.83-1.20	2.83-1.20
5	2.90-1.20	2.83-1.20	2.83-1.20
5-CH_3	0.95-0.81	0.95-0.83	0.95-0.83
6	2.90-1.20	2.83-1.20	
7	3.44-3.52, 1H	3.43-3.49, 1H	3.44-3.49, 1H
8	2.90-1.20	0.95-0.83	2.83-1.20
8-CH_3	1.03, 3H, d (6.1)	1.03, 3H, d (5.9)	1.01, 3H
9	4.42, 1H, br s	4.53, 1H	4.48, 1H, br s
9-OCH_3	3.52, 3H, s	3.09, 3H, s	3.15, 3H, s
10	-	-	-
11	7.61, 1H, d (1.2)	7.57, 1H, s	7.64, 1H, s
12	-	-	-
13	-	-	-
14	8.10, 1H, s	8.07, 1H, s	8.10, 1H, s
15	-	-	-
16	-	-	-
17	8.04, 1H, s	8.03, 1H, s	8.06, 1H, s
18	-	-	-
19	6.29, 1H, d (16.0)	6.29, 1H, d (16.3)	6.31, 1H, d (15.4)
20	7.51, 1H, ddd (16.0, 10.0, 5.9)	7.53, 1H, m	7.51, 1H, m
21	2.90-1.20	0.95-0.83	
22	3.72, 1H, m	3.71, 1H, m	3.65, 1H, m
22-OCH_3	3.44, 3H, s	3.43, 3H, s	3.43, 3H, s

Table 13 (continued)

Position	δ_H (ppm), mult. (*J* in Hz)		
	[56]	[57]	[58]
23	2.90-1.20	2.83-1.20	2.83-1.20
23-CH_3	0.95-0.81	0.95-0.83	0.95-0.83
24	5.14, 1H, m	5.14, 1H, m	5.13, 1H, m
25	2.90-1.20	2.83-1.20	2.83-1.20
26	2.99, 1H	3.00, 1H	2.99, 1H
26-OCH_3	3.33, 3H, s	3.32, 3H, s	3.33, 3H, s
27	2.90-1.20	2.83-1.20	2.83-1.20
27-CH_3	0.95-0.81	0.95-0.83	0.95-0.83
28	2.90-1.20	2.83-1.20	2.83-1.20
29	2.90-1.20	2.83-1.20	2.83-1.20
30	-	-	-
31	2.90-1.20	2.83-1.20	2.83-1.20
31-CH_3	0.95-0.81	0.95-0.83	0.95-0.83
32	3.32-3.34, 1H	3.32-3.34, 1H	3.30-3.35, 1H
32-OCH_3	3.34, 3H, s	3.34, 3H, s	3.35, 3H, s
33	2.90-1.20	2.83-1.20	2.83-1.20
33-CH_3	1.16, 3H, d (7.1)	1.16, 3H, d (6.5)	1.16, 3H, d (6.5)
34	5.10, 1H, m	5.12, 1H, m	5.10, 1H, m
35	6.46 [7.13], 1H, d (14.3)	6.46 [7.13], 1H, d (14.5)	6.46 [7.13], 1H, d (14.2)
35-NCH_3	3.04 [3.08], 3H, s	3.04 [3.08], 3H, s	3.04 [3.08], 3H, s
35-NCHO	8.27 [8.08], 1H, s	8.29 [8.07], 1H, s	8.29 [8.07], 1H, s
Triazole 4	-	-	-
Triazole 5	-	7.41, 1H, s	7.49, 1H, s
$NHCH_2$	-	4.53, 2H	4.01, 2H, s
NH	-	5.47, 1H, m	-
Fmoc 1	-	7.58, 1H, d (7.2)	-
Fmoc 2	-	7.30, 1H, t (7.2)	-
Fmoc 3	-	7.40, 1H, t (7.2)	-
Fmoc 4	-	7.76, 1H, d (7.2)	-
Fmoc 4a	-	-	-

Table 13 (continued)

Position	δ_H (ppm), mult. (*J* in Hz)		
	[56]	[57]	[58]
Fmoc 4b	-	-	-
Fmoc 5	-	7.76, 1H, d (7.2)	-
Fmoc 6	-	7.40, 1H, t (7.2)	-
Fmoc 7	-	7.30, 1H, t (7.2)	-
Fmoc 8	-	7.58, 1H, d (7.2)	-
Fmoc 8a	-	-	-
Fmoc 9	-	4.22, 1H, t (7.2)	-
Fmoc 9a	-	-	-
Fmoc CO	-	-	-
Fmoc CH_2	-	4.40, 2H, d (7.2)	-

Chemical shifts for minor conformer are in brackets.

Table 14 The ^{13}C NMR spectral data of 7-azidokabiramide C **[56]**, 7-[4-*N*-(9*H*-fluoren-9-yl-methoxycarbonyl)aminomethyl-1,2,3-triazol-1-yl]kabiramide C **[57]**, and 7-(4-aminomethyl-1*H*-1,2,3-triazol-1-yl)kabiramide C **[58]**.

Position	δ_c (ppm)		
	[56]	[57]	[58]
1	171.57	171.68	171.67
2	42.46[a]	42.59[a]	42.64[a]
3	69.25	69.48	69.52
3-$OCONH_2$	157.19	157.09	156.14
4	42.89[a]	42.59[a]	41.97[a]
5	25.56	26.15	26.46
5-CH_3	20.92	20.96	21.72
6	39.51[a]	39.89[a]	40.13[a]
7	64.42	62.23	62.19
8	38.56[b]	42.37[b]	42.43[b]
8-CH_3	6.23	6.81	6.97
9	82.39	80.71	80.81
9-OCH_3	58.50	58.09	58.29
10	142.35	144.53	142.28
11	135.52	135.48	135.44
12	155.50	155.48	155.52
13	131.00	130.94	131.11
14	136.70	136.94	136.98
15	156.28	156.36	156.44
16	129.80	129.73	129.86
17	137.11	137.37	137.36
18	163.13	163.19	163.26
19	115.31	115.63	115.70
20	142.04	141.93	141.82
21	33.65	33.67	33.77
22	78.98	79.40	79.48
22-OCH_3	57.32	57.38	57.43
23	40.36[b]	40.24[b]	40.38

Table 14 (continued)

Position	δ_C (ppm)		
	[56]	[57]	[58]
23-CH_3	8.43	8.64	8.44
24	73.87	73.90	73.94
25	32.81	32.28	32.40
26	81.95	81.89	81.96
26-OCH_3	57.77	57.93	57.97
27	34.42 [34.47]	34.35	34.41
27-CH_3	15.45	15.53	15.56
28	24.81	24.72	24.77
29	42.34 [42.26]	42.37	42.43
30	214.07 [214.16]	214.11 [214.20]	214.15 [214.25]
31	48.97 [49.05]	49.03 [49.12]	49.07 [49.16]
31-CH_3	13.48	13.54	13.57
32	87.21 [87.28]	87.24 [87.33]	87.28 [87.38]
32-OCH_3	61.28	61.32	61.36
33	37.35 [37.54]	37.37 [37.59]	37.32 [37.43]
33-CH_3	19.27	19.31	19.35
34	111.22 [113.02]	111.28 [113.06]	111.32 [113.11]
35	128.66 [124.66]	128.70 [124.68]	128.75 [124.74]
35-NCH_3	27.51 [33.03]	27.56 [33.08]	27.60 [33.12]
35-NCHO	162.08 [160.80]	162.13 [160.85]	162.16 [160.87]
Triazole 4	-	141.93	142.28
Triazole 5	-	121.27	120.33
$NHCH_2$	-	36.66	42.38
Fmoc 1	-	127.63	-
Fmoc 2	-	125.03	-
Fmoc 3	-	119.91	-
Fmoc 4	-	126.97	-
Fmoc 4a	-	141.19	-
Fmoc 4b	-	141.19	-
Fmoc 5	-	126.97	-

Table 14 (continued)

Position	δ_c (ppm)		
	[56]	[57]	[58]
Fmoc 6	-	119.91	-
Fmoc 7	-	125.03	-
Fmoc 8	-	127.63	-
Fmoc 8a	-	143.81	-
Fmoc 9	-	47.11	-
Fmoc 9a	-	143.81	-
Fmoc CO	-	156.36	-
Fmoc CH_2	-	66.89	-

Chemical shifts for minor conformer are in brackets.

[a-b]Assignments may be interchanged within column.

3. Synthesis of the fluorescent derivatives of kabiramide C

On the basis of previous studies (Klenchin et al., 2003; Tanaka et al., 2003), we reasoned that fluorescent moieties introduced into kabiramide C *via* the 7-hydroxy would face the solvent and therefore not interfere with the binding property of kabiramide C to G-actin. We elected to synthesize the key intermediate, AMT-KabC from kabiramide C. The long linker between C-7 of kabiramide C and the fluorescent moieties should minimize effects of the bulky probe on actin binding. Furthermore, the introduction of a terminal amino group on kabiramide C allowed for the facile synthesis of optical probe derivatives using commercially available succinimidyl ester probes, including succinimidyl esters of tetramethylrhodamine (TMR), rhodol green (RG), IC5, fluorescein diester (FDE), and dapoxyl (DAP). The structures of the fluorescent dyes are shown in Figure 26.

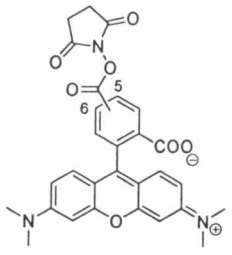

5(6)-Carboxytetramethylrhodamine, succinimidyl ester

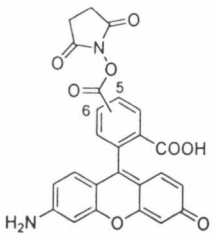

Rhodol Green carboxylic acid, succinimidyl ester

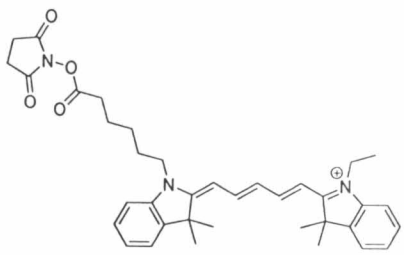

IC5-OSu

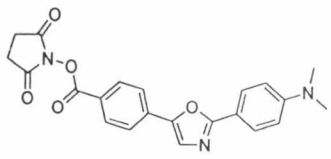

Dapoxyl carboxylic acid, succinimidyl ester

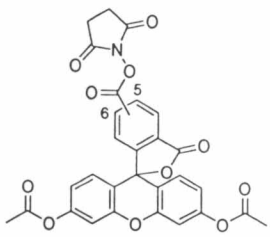

5(6)-carboxyfluorescein diacetate *N*-succinimidyl ester

Figure 26 Structures of the fluorescent dyes.

The couple reactions between AMT-KabC and fluorescent dyes were performed smoothly by using the amine-reactive fluorescent dyes that have succinimide functional group. The synthetic procedure of fluorescent kabiramide C probes is shown in Figure 27 and the acylation reaction mechanism was proposed in Figure 28. The reaction products, fluorescent kabiramide probes, were determined by using ESI mass spectral data and UV spectral data.

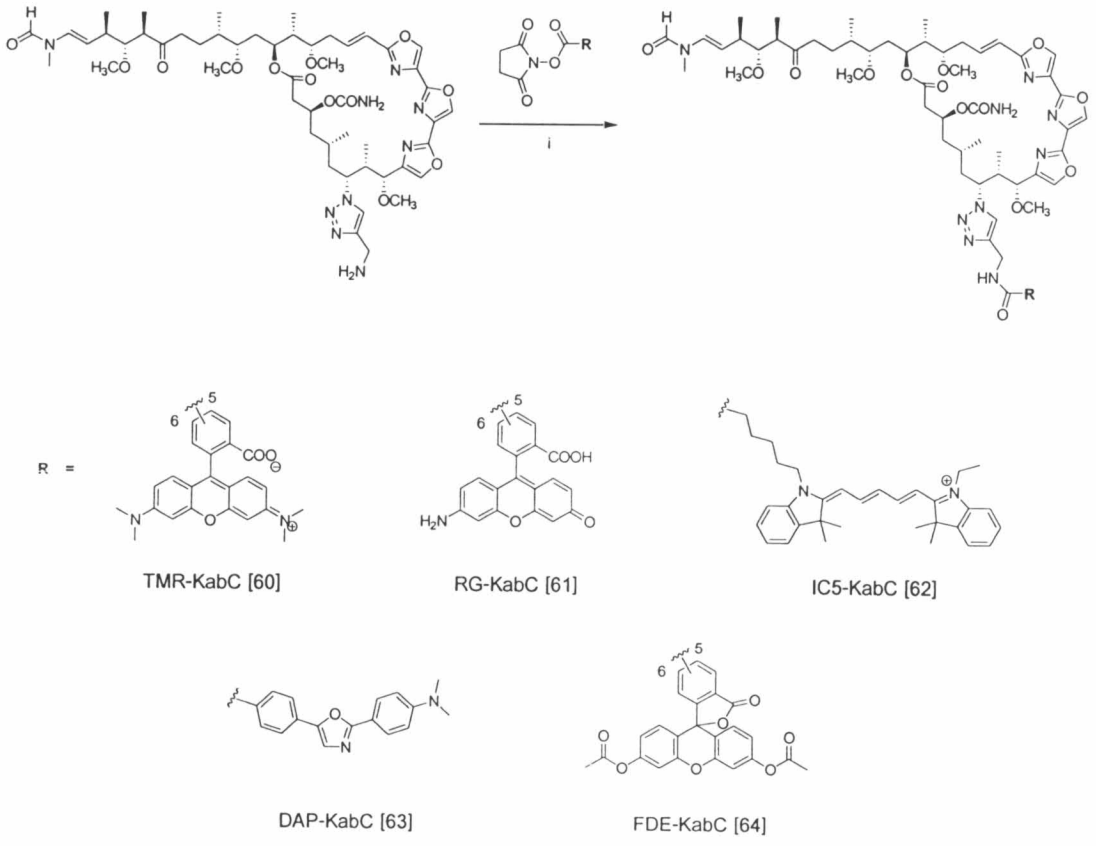

Figure 27 Synthesis of fluorescent kabiramide C probes: (i) CH_2Cl_2/DMSO, rt.

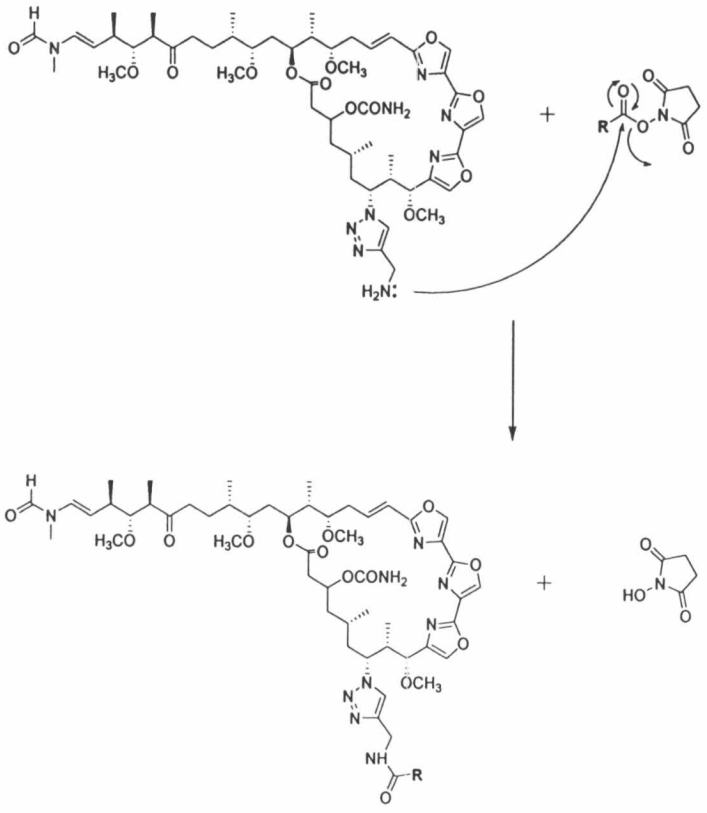

Figure 28 Proposed mechanism of acylation reaction of 7-(4-aminomethyl-1*H*-1,2,3-triazol-1-yl)kabiramide C

3.1 TMR-KabC

The AMT-KabC was coupled to 5-(and 6)-carboxytetramethyl-rhodamine succinimidyl ester to give a red amorphous solid of tetramethyrhodamine derivative **[60]** (TMR-KabC). This compound has molecular formula $C_{76}H_{95}N_{11}O_{17}$ corresponding to the presence of pseudomolecular ion peak at *m/z* 1456.6838 $[M+Na]^+$ in the ESI mass spectrum (Figure 90). The UV spectrum (Figure 91) also confirmed the presence of kabiramide (236 and 251 nm) and tetramethylrhodamine (545 nm) in its structure.

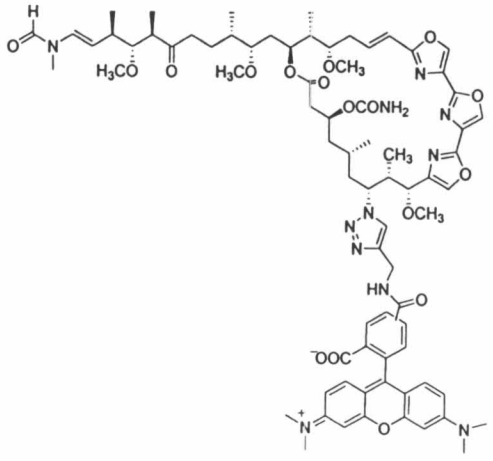

Figure 29 The structure of TMR-KabC.

3.2 RG-KabC

The Rhodol green derivative **[61]** (RG-KabC) was obtained as a green amorphous solid from the reaction of AMT-KabC and rhodol green carboxylic acid succinimidyl ester. The ESI mass spectrum (Figure 92) showed the pseudomolecular ion peak at *m/z* 1401.6028 $[M+Na]^+$ indicating the molecular formula of $C_{72}H_{86}N_{10}O_{18}$. The UV spectrum (Figure 93) exhibited the absorption at λ_{max} 245 and 494 nm indicating the presence of kabiramide and rhodol green, respectively.

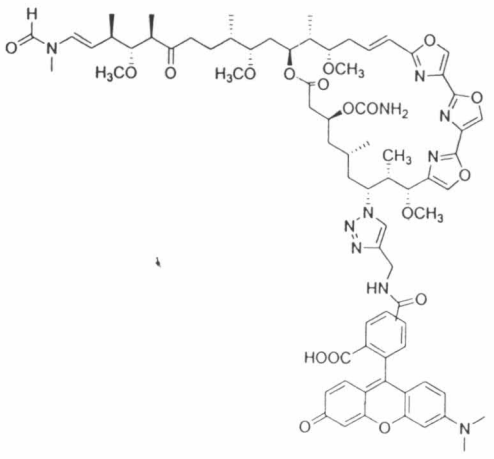

Figure 39 The structure of RG-KabC.

3.3 IC5-KabC

The reaction of AMT-KabC and IC5-OSu gave a blue amorphous solid of IC5 derivative **[62]** (IC5-KabC). This compound has molecular formula $C_{84}H_{114}N_{11}O_{14}$ that was confirmed by the presence of pseudomolecular ion peak at *m/z* 1501.8665 $[M+H]^+$ in ESI mass spectrum (Figure 94). The UV spectrum (Figure 95) revealed the absorption of kabiramide and IC5 at λ_{max} 245 and 643 nm, respectively.

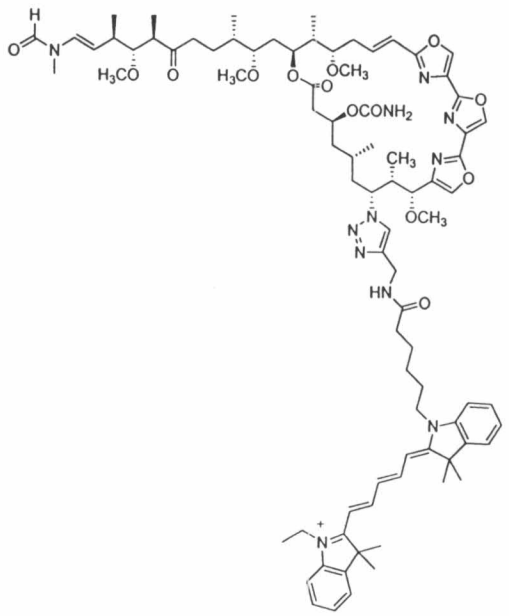

Figure 31 The structure of IC5-KabC.

3.4 DAP-KabC

AMT-KabC was coupled to dapoxyl carboxylic acid succinimidyl ester to give the dapoxyl derivative **[63]** (DAP-KabC) as a white amorphous solid. The ESI mass spectrum (Figure 96) showed the pseudomolecular ion peak at *m/z* 1334.6503 $[M+Na]^+$ implying the molecular formula of $C_{69}H_{89}N_{11}O_{15}$. The UV spectrum (Figure 97) exhibited the absorption of kabiramide and IC5 at λ_{max} 247 and 370 nm, respectively.

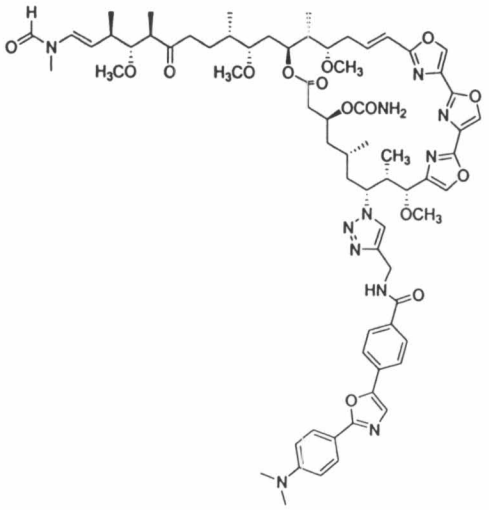

Figure 32 The structure of DAP-KabC.

3.5 FDE-KabC

FDE-KabC **[64]**, a white amorphous solid, was synthesized by the reaction of AMT-KabC and 5(6)-carboxyfluorescein diacetate *N*-succinimidyl ester. The pseudomolecular ion peak at *m/z* 1486.6056 $[M+Na]^+$ in ESI mass spectrum (Figure 98) confirmed the molecular formula of $C_{76}H_{89}N_9O_{21}$ of this compound. The UV spectrum (Figure 99) presented the absorption at 245 nm implying the presence of kabiramide.

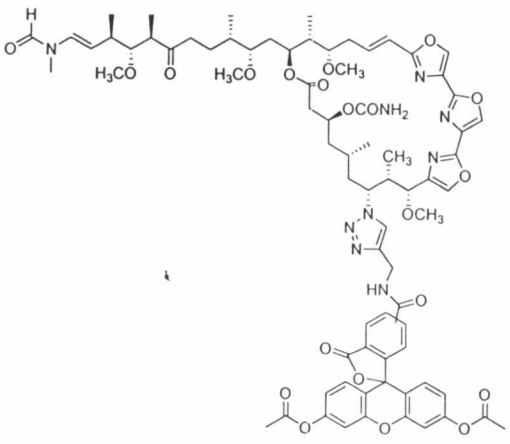

Figure 33 The structure of FDE-KabC.

4. Actin-binding properties

The kabiramides in this study can be separated into two groups: non-fluorescent kabiramides and fluorescent kabiramides. The actin-binding properties of non-fluorescent kabiramide were determined by the measurement of fluorescence intensity of prodan-G-actin as a function of kabiramide. The interactions of the fluorescent kabiramide C probes and G-actin were characterized by measuring fluorescence intensity (FI), fluorescence resonance energy transfer (FRET), iodide quenching and fluorescence anisotropy (FA).

4.1 Actin-binding properties of the non-fluorescent kabiramides

The group of non-fluorescent kabiramides consists of kabiramides C, D, and F, 7-azido kabiramide C, 7-[4-*N*-(9*H*-fluoren-9-yl-methoxycarbonyl)amino-methyl-1,2,3-triazol-1-yl]kabiramide C, and 7-(4-aminomethyl-1*H*-1,2,3-triazol-1-yl) kabiramide C. The actin-binding property of these compounds was determined by titrating 1 μM prodan G-actin with increasing amounts of the tested compounds from 0.1 to 2 μM. The stoichiometric binding of the tested compounds to G-actin was determined at the reach of steady state. Previous study (Tanaka et al., 2003) reported that addition of up to 2% methanol to prodan-G-actin had no effect on the emission spectrum or polymerization kinetics.

It is known that the amino acid residues close to Cys-374 in actin are engaged in specific interactions of barbed end capping proteins and gelsolin (Doi et al., 1991). Therefore, measurement of fluorescence emission of the probe attached to Cys-374 of actin could provide the information on molecular complex of actin with actin-binding proteins or drugs.

The environment sensitive probe, acrylodan, was covalently bound to Cys-374 of actin to give prodan-G-actin. The fluorescence emission spectrum of prodan-G-actin in G-buffer exhibited the maximal emission wavelength at 496 nm and shifted to 465 nm when polymerization to prodan-F-actin occurred. In contrast, the

binding of kabiramide C to prodan-G-actin decreased the prodan fluorescence intensity and shifted the maximum emission from 496 nm to 510-520 nm (Marriott et al., 1988; Tanaka et al., 2003). This evidence is used to determine the actin-binding properties of kabiramides.

The stoichiometric binding of all kabiramides including kabiramides C, D, and F, 7-azido kabiramide C, 7-[4-*N*-(9*H*-fluoren-9-yl-methoxycarbonyl)aminomethyl-1,2,3-triazol-1-yl] kabiramide C, and 7-(4-aminomethyl-1*H*-1,2,3-triazol-1-yl) kabiramide C was 1:1 by the analysis of decreased fluorescence intensity of prodan-G-actin as the amount of the tested compounds was increased as shown in Figures 100, 101, 102, 103, 104, and 105, respectively.

4.2 Actin-binding properties of fluorescent kabiramides

4.2.1 TMR-KabC

The integration of fluorescence emission spectra of the TMR-KabC unchanged upon binding to unlabeled G-actin (Figure 106A). This result suggested that the molecular environment of the TMR group is similar in both the free and bound states and that the linker is sufficiently constrained by the triazole ring to prevent interactions between the polar TMR group with the protein. However, the binding of TMR-KabC to G-actin substantially increased the hydrodynamic volume of the bound TMR-KabC compared to the free TMR-KabC. This change was accurately quantified by measuring the steady state FA (Yan and Marriott, 2003) of the free TMR-KabC and increasing amount of unlabeled G-actin (Figure 106B). The FA values increased linearly under the stoichiometric binding condition and analysis of the FA data shows that TMR-KabC bound to G-actin in a 1:1 complex (Figure 106B). Further support for this conclusion was provided in a FRET study of the interaction between TMR-KabC and Prodan (Cys-374) labeled G-actin shown in Figure 106C. Excitation of Prodan on G-actin generated a strong fluorescence center at 496 nm that decreased significantly upon adding increasing amounts of TMR-KabC, which was caused by KabC mediated quenching and by FRET from Prodan to TMR-KabC, which was also seen by the sensitization of

TMR fluorescence. Analysis of the increase in TMR fluorescence confirmed that TMR-KabC bound to G-actin in a 1:1 complex (Figure 106D).

It has been shown that the quantum yield of the TMR emission and the lifetime of excited state are constant in the free and bound states. Thus, the change in FA value of TMR-KabC is directly related to the fractions of the probe in a sample that exist in the free state (r of 0.056±0.002) and the G-actin bound state (r of 0.236±0.002) according to the equation: $r = F_f r_f + F_b r_b$, where as $F_f + F_b = 1$, r is the observed FA value, F_f and F_b are fractions of free and bound fluorescent ligand, and r_f and r_b are FA of free and bound fluorescent ligand, respectively. The relatively low FA value (0.236± 0.002) found for TMR-KabC in the G-actin complex suggested that the TMR group experienced a considerable degree of local motion. Furthermore, the FA value was unchanged when the TMR-KabC-G-actin complex was added at a sub-stoichiometric level to a polymerizing solution of actin, where it formed TMR-KabC capped, barbed-ends (Tanaka et al., 2003). These results supported our view that the TMR probe in both G-and F-actin is fully exposed to the solvent where it experiences considerable rotational freedom.

To learn more about the molecular environment of the TMR groups in its G-actin complex, we performed a potassium iodide mediated collision quenching study. The quenching curves for free and bound TMR-KabC showed two quenching modes with the faster rate accounting for the greater degree of quenching. Analysis of the rapid quenching mode was achieved by restricting the linear regression of fluorescence quenching data to 60 mM KI (Figure 108). Free TMR-KabC was found to exhibit collision molar quenching constants of 29.6 M^{-1} (R^2 of 0.999). This corresponding value for TMR-KabC bound to G-actin was 13.5 M^{-1} (R^2 of 0.929). Given a fluorescence lifetime for TMR-KabC of 4 ns (Heidecker et al., 1995), the unbound probe was calculated to be quenched at 7.4×10^9 $M^{-1}s^{-1}$, which is very close to the diffusion controlled rate of 8×10^9 $M^{-1}s^{-1}$ (Marriott et al., 1988). Since the lifetimes of the TMR-KabC did not change on binding to G-actin, the quenching rate constants calculated for the bound probe was at 3.38×10^9 $M^{-1}s^{-1}$. The analysis of these quenching data supported the conclusion reached from the spectral and FA analyses, showing that the

TMR-KabC probe is fully exposed to the solvent and experience a considerable degree of rotational freedom.

4.2.2 RG-KabC

The rhodol green derivative of KabC exhibited an excitation spectrum centered at 488 nm and emission at 517 nm. The fluorescence spectrum of RG-KabC did not change upon binding to G-actin (Figure 107A), which suggested that the molecular environments of the probe in the free and bound states were similar. The FA value of RG-KabC changed from a value of 0.036±0.001 in the free-state to 0.180±0.003 when bound to G-actin (Figure 107B). As seen with TMR-KabC, this anisotropy value suggested that the probe exhibits considerable rotational freedom when bound to G-actin and confirms the suggestion that the short linker between the C-7 of KabC and the probe prevents the RG group from interacting with the protein. The similarity of the molecular environments for the RG-KabC within G-actin and capped to the (+)-end of actin filaments was implied from the unchanged FA value of RG-KabC in these two preparations. The higher degree of spectral overlap between Prodan emission on G-actin and the absorption spectrum of RG-KabC resulted in efficient FRET process (Figure 107C-D), which can be used to determine properties of the interaction including the formation of a 1:1 complex.

An iodide quenching experiment of RG-KabC also showed the similar results as seen in TMR-KabC. This study suggested that RG-KabC probe is fully exposed to the solvent. Analysis of the rapid quenching mode was achieved by restricting the linear regression of fluorescence quenching data to 60 mM KI (Figure 108). Analysis of Stern-Volmer plot showed that free RG-KabC probe has collision molar quenching constants of 22.5 M^{-1} (R^2 of 0.976). This value for RG-KabC bound to G-actin was 14.5 M^{-1} (R^2 of 0.914). The quenching rate constants calculated for the free and bound probes were 5.6×10^9 $M^{-1}s^{-1}$ and 3.63×10^9 $M^{-1}s^{-1}$, respectively if we assume the fluorescence lifetime of RG is 4 ns (Heidecker et al., 1995).

4.2.3 IC5-KabC

The relative fluorescence quantum yield of IC5-KabC increased ~20% upon binding to G-actin and did not involve any significant spectral shift (Figure 109A-B). Steady state FA measurements of IC5-KabC increased from 0.155±0.005 in the free-state to 0.331±0.002 when stoichiometrically bound to G-actin (Figure 109C). Both the integrated fluorescence intensity of the emission spectrum and the FA value were increased linearly with increasing G-actin concentration. The analysis of these data showed that IC5-KabC bound stoichiometrically (1:1) to G-actin. This result was confirmed from a FRET based analysis of Prodan-actin emission at 485 nm as function of IC5-KabC concentration (Figure 109D-E). Since the FA value for IC5-KabC bound to the terminal protomer at the (+)-end of an actin filament did not increase compared to the G-actin complex, ascribable the small difference in the FA of the IC5-KabC-G-actin complex (0.331) from the limiting anisotropy (0.4) in terms of a low amplitude local motion of the IC5-KabC within the complex.

The high value of the steady state FA for IC5-KabC compared to that for the RG- and TMR-KabC probes on actin is expected if: (a) the lifetime of IC5-KabC in the G-actin complex was short compared to the RG-KabC and TMR-KabC bound probes or (b) if the longer link between the IC5 group and the C-7 of KabC allows the IC5 probe to double back and engage in interactions with the protein surface that restrict local motion. Since the relative quantum yield of IC5-KabC emission is high, and actually increases by ~20% in the bound versus free states, then the fluorescence lifetime would if anything increase on binding to G-actin - on the basis of this argument it is possible to rule out the first possibility. On the other hand, the emission spectrum of the IC5 probe (Mujumdar et al., 1993) is slightly red shifted in the G-actin complex compared to the free probe, which is evidence that the probe engages in different interactions in the G-actin complex compared to water. Taken together, proposed that the very high FA value measured for IC5-KabC bound G-actin results from a significant reduction in local motion of the probe brought about by interactions between the IC5 probe and the G-actin.

4.2.4 DAP-KabC

Dapoxyl group has been reported to be sensitive to changes in its molecular environment and accordingly the relative fluorescence quantum yield of DAP-KabC decreased on binding to G-actin. The fluorescence of DAP-KabC was severely quenched in the complex with G-actin (Figure 110A). These data were used to determine the actin-binding property of DAP-KabC. Analysis of the decreased fluorescence intensity of DAP-KabC as the increase amounts of G-actin showed that DAP-KabC binds to G-actin in a 1:1 complex (Figure 110B).

4.2.5 FDE-KabC

The binding of the non-fluorescent FDE-KabC probe to G-actin was confirmed by monitoring the emission ratio of Prodan-actin and FDE-KabC at 485 and 520 nm as a function of FDE-KabC concentrations. Excitation of the Prodan fluorophore in G-actin led to a strong emission centered at 496 nm that decreases upon the addition of increasing amount of FDE-KabC due to KabC mediated quenching of Prodan fluorescence and the donor quenching and FDE sensitized emission due to FRET (Figure 111A). Analysis of these data confirmed that the FDE-KabC probe binds to G-actin in a 1:1 complex (Figure 111B).

5. Live cell imaging of TMR-KabC and FDE-KabC

The FDE-KabC optical probe has three key features that make it suitable for *in vivo* imaging studies: (1) the probe readily permeates the plasma membrane of living cells; (2) the fluorescein is non-fluorescent until one or both acetate groups are hydrolyzed by intracellular esterases; and (3) once cleaved the FDE-KabC probe remains trapped within the cell.

Cells treated with medium containing 100 nM FDE-KabC display robust fluorescence within a few minutes. Confocal imaging of FDE-KabC within live NIH-3T3 cells showed two categories of staining. The first was a diffuse fluorescence that

associates with FDE-KabC-G-actin existing in complex with G-actin sequestering proteins such as thymosin β4 (Roy et al., 2001); the second was far more intense of FDE-KabC-G-actin in actin filament and was found at the cell cortex, especially at sites of cell protrusion (Figure 34A).

The brilliantly fluorescent TMR-KabC also crossed the plasma membrane where it becomes trapped within the cytoplasm. After washing cells with fresh medium, fluorescence imaging also showed that the distribution of the entrapped probe is similar to that described for FDE-KabC (Figure 34B). The red-shifted excitation and emission spectra of the TMR probe together with its increased photostability generate images that are of higher contrast than FDE-KabC.

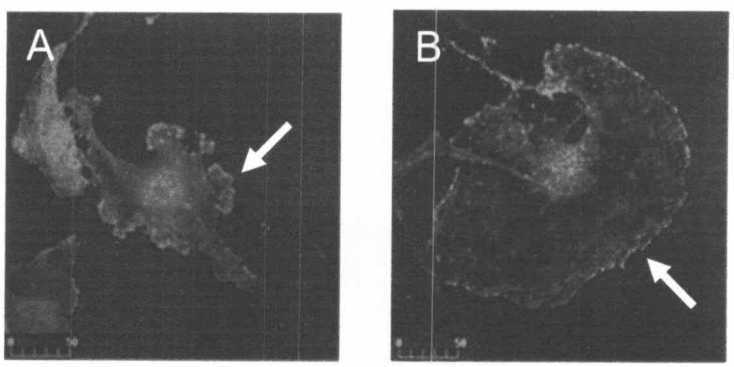

Figure 34 Confocal images of FDE-KabC-G-actin (A) and TMR-KabC-G-actin (B) in actin filament at protrusion site (arrow) of live NIH 3T3 cells.

The other three fluorescent kabiramides, RG- KabC, IC5-KabC, and DAP-KabC, were tested in living NIH 3T3 cells. All of them also penetrated into the cells and showed the labeling as described in FDE-KabC and TMR-KabC. However, these three derivatives are not suitable for using to probe actin within cells because: (1) RG-KabC slightly penetrated into the cells, (2) most of IC5-KabC were trapped within vesicles, and (3) the fluorescence intensity of DAP-KabC was decreased when it bound to G-actin (data not shown).

6. Biological activities

6.1 Antifungal activity

The antifungal activity against *C. albicans* was tested for the three isolated kabiramides C, D, and F. All of them exhibited equal potency according to the presence of clear zone with the diameter of 22 mm at the concentration of 100 µg/disc.

6.2 Cytotoxic activity

Only AMT-KabC was tested for the cytotoxic activity against HeLa cells. HeLa cells were examined at three concentrations of AMT-KabC (10, 100, and 1000 nm). The images of cells were taken after treatment with the tested compound for 16 hours. Cells treated with 10 nm of AMT-KabC (Figure 35B) showed an increase in binucleated cells when compared with the control (Figure 35A) because of the cytokinesis arrest that usually observed in actin-active agents. At 100 nm (Figure 35C), cells showed a loss of actin-associated cell-cell contacts, a loss of cell motility, existence of cell blebbling, and some were dead. Cells treated with AMT-KabC at the concentration of 1000 nm had a complete breakdown of their cytoskeleton and died (Figure 35D).

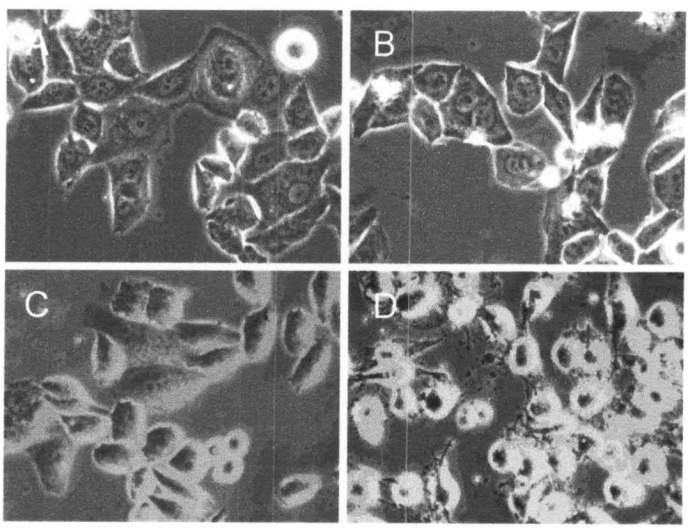

Figure 35 Effect of AMT-KabC on HeLa cells. The images of HeLa cells were taken after 16 h of drug treatment. The concentrations of AMT-KabC are as follows: control (A), 10 nM (B), 100 nM (C), and 1000 nM (D).